A simple and fast phase transition relaxation solver for compressible multicomponent two-phase flows

Alexandre Chiapolino[a,b], Pierre Boivin[1b], Richard Saurel[a,b,c]

[a] *RS2N, Chemin de Gaumin, 83640 Saint-Zacharie, France*
[b] *Aix Marseille Univ., CNRS, Cent. Marseille, M2P2 UMR 7340, 13451, Marseille, France*
[c] *University Institute of France*

Abstract

The present paper aims at building a fast and accurate phase transition solver dedicated to unsteady multiphase flow computations. In a previous contribution (Chiapolino 2016), such a solver was successfully developed to compute thermodynamic equilibrium between a liquid phase and its corresponding vapor phase. The present work extends the solver's range of application by considering a multicomponent gas phase instead of pure vapor, a necessary improvement in most practical applications. The solver proves easy to implement compared to common iterative procedures, and allows systematic CPU savings over 50%, at no cost in terms of accuracy. It is validated against solutions based on an accurate but expensive solver. Its capability to deal with cavitating, evaporating and condensing two-phase flows is highlighted on severe test problems both 1D and 2D.

Keywords: multiphase flows, interfaces, hyperbolic systems, relaxation, phase transition.

Introduction

Phase transition between liquid and gas phases is a well-established phenomenon, which tends to relax thermochemical potentials towards equilibrium. Yet, finding the thermodynamic equilibrium can be tedious, as the corresponding equations are non-linear, the culprit being the non-trivial relation linking pressure (p) and temperature (T) at saturation. In multiphase compressible flows modeling, phase transition has dominant effects in many applications, and has to be accounted for via appropriate phase transition models. Iterative equilibrium solvers are

[1]Corresponding author: `pierre.boivin@univ-amu.fr`

usually computationally expensive, as they require complex root-finding procedures, sometimes draining more CPU time than the flow computation itself. Their coding is not straightforward, as for example, simple phase bounds require special attention.

Our previous work [1] presented a robust, fast and accurate alternative to the exact equilibrium solver in the case of flows consisting of a liquid phase in equilibrium with its own vapor. Speedup on the order of 50% were achieved on computations of such flows. When only liquid and the corresponding vapor are present, p and T are necessarily bound by the saturation curve $p = p_{sat}(T)$, simplifying somewhat the equations.

In the present paper, we aim at extending the model to liquid in equilibrium with multi-component gases. In this case, p and T are not directly on the saturation curve, but are related through the partial pressure of the vapor component in the multi-component gas phase. This allows the well-known existence of liquid vapor in air at atmospheric conditions, albeit a temperature below the boiling point.

The range of flow solvers to which the present model applies is identical to its previous version: it is designed in association with non-equilibrium hyperbolic flow models, such as Baer and Nunziato's (1986) [2] and its reduced versions. This includes the 5-equation model of Kapila et al. (2001) [3] and its extension for cavitating flows [4–6], as well as temperature equilibrium version as the Homogeneous Relaxation Model (HRM) and Homogeneous Equilibrium Model (HEM) [7, 8].

This paper is organized as follows. The first two sections remind the 4-equation flow model [6] and the corresponding thermodynamic closure, backbone of the present study. The 4-equation two-phase model is indeed the simplest flow model for the relaxation solver. Also, a wide range of applications can be addressed with this approach [6]. The third section presents the system of equation to be solved to relax thermochemical potentials, while the fourth details how to do so. The last sections are dedicated to displaying and validating the algorithm capabilities, through a series of 1D and 2D cavitating, evaporating and condensing test cases.

1. Flow model

1.1. Classical two-phase flow model

The phase transition relaxation solver may be used with models mentioned previously (with 7, 5, 4 and 3 partial differential equations) but its presentation is simplified in the context of the 4-equation model (often called HRM). When dealing with more sophisticated formulations, for example the 7-equation model, extra ingredients have to be presented, such as velocity and pressure relaxation solvers for example [9, 10]. Here, there is a single step that makes the connection from the 4-equation model (modeling mixtures out of thermodynamic equilibrium) and the 3-equation model (mixtures in full equilibrium). The classical 4-equation model for a two-phase flow reads:

$$\begin{cases} \dfrac{\partial \rho}{\partial t} + div(\rho \mathbf{u}) & = 0, \\ \dfrac{\partial \rho \mathbf{u}}{\partial t} + div\left(\rho \mathbf{u} \otimes \mathbf{u} + p\underline{\underline{I}}\right) & = 0, \\ \dfrac{\partial \rho E}{\partial t} + div\left((\rho E + p)\mathbf{u}\right) & = 0, \\ \dfrac{\partial \rho_l \alpha_l}{\partial t} + div(\rho_l \alpha_l \mathbf{u}) & = 0, \end{cases} \tag{1.1}$$

where the liquid mass conservation equation can be written alternatively as,

$$\frac{\partial \rho Y_l}{\partial t} + div(\rho Y_l \mathbf{u}) \quad = 0. \tag{1.2}$$

Here $Y_{l,g}$, $\alpha_{l,g}$, $\rho_{l,g}$ denote respectively the mass fraction, the volume fraction and the material density of the liquid (l subscript) and gas (g subscript) phases. ρ represents the mixture density, $\mathbf{u}$ represents the mixture center of mass velocity, p denotes the mixture pressure and E the mixture total energy ($E = e + u^2/2$). The mixture specific internal energy is defined as $e = Y_l e_l + Y_g e_g$. Mass transfer has been omitted in system (1.1) as it is addressed later.

1.2. Extension to a multicomponent gas phase

Considering multicomponent effects in the gas phase needs additional mass balance equations that can be written as,

$$\frac{\partial \rho_g \alpha_g y_k}{\partial t} + div(\rho_g \alpha_g y_k \mathbf{u}) \quad = 0, \tag{1.3}$$

where y_k denotes the k-th gas component mass fraction within the gas phase. In the thermodynamic closure considered in this study, and detailed in the next section, the gas phase is assumed to follow the ideal gas equation of state. In addition, the two-phase mixture evolves in both mechanical and thermal equilibrium.

Many multiphase flow solvers can natively handle an arbitrary number of phases, each occupying its own volume, but not necessarily a multi-component gas phase. Because the molar volume is independent on the gas constituent, it is equivalent to consider a multicomponent gas phase (ideally mixed) – in which case the gas constituents mass balance equations follow Eq. (1.3) – or assume that each component in the gas phase occupies its own volume (as a pure constituent). The equivalence between the two formalisms is clarified in the next section. When each gas constituent is assumed to occupy its own volume, all mass balance equations can be written as:

$$\frac{\partial \rho Y_k}{\partial t} + div(\rho Y_k \mathbf{u}) \quad = 0,$$

where the subscript k can refer to the liquid phase, or a gas constituent mass conservation. In all following Sections:

- $k = 1$ for the liquid,
- $k = 2$ for the gas component corresponding to species 1 vapor,
- $k = 3, \ldots, N$ for the remaining gas components, considered non-condensable in this work.

This notation for the species conservation equation is more convenient, as Y_k is now the volume fraction for the k-th species in the entire control volume (containing both liquid and gas phases), so that the conservation equation for each species within the gas phase is of the same form as the liquid mass conservation equation.

The extended two-phase flow model consequently reads,

$$\begin{cases} \dfrac{\partial \rho}{\partial t} + div(\rho \mathbf{u}) & = 0, \\ \dfrac{\partial \rho \mathbf{u}}{\partial t} + div\left(\rho \mathbf{u} \otimes \mathbf{u} + p\underline{\underline{I}}\right) & = 0, \\ \dfrac{\partial \rho E}{\partial t} + div\left((\rho E + p)\mathbf{u}\right) & = 0, \\ \dfrac{\partial \rho Y_k}{\partial t} + div(\rho Y_k \mathbf{u}) & = 0, \end{cases} \tag{1.4}$$

with

$$E = e + \frac{1}{2}\mathbf{u} \otimes \mathbf{u}, \quad e = \sum_{k=1}^{N} Y_k e_k,$$

System (1.4) is clearly reminiscent of the reactive (or multicomponent) Euler equations widely used in chemically reacting flows. However, the thermodynamic closure differs significantly from the one used in gas mixtures and is addressed hereafter.

2. Thermodynamic closure

This section presents the equations of state (EOS) used for each pure component as well as the mixture equation of state. Preliminarily, let us demonstrate the equivalence between considering a gas phase ideally mixed, following Dalton's law, and a gas phase in which each constituent is assumed to occupy its own volume, in the specific context of temperature and pressure equilibrium.

2.1. The gas phase is ideally mixed: Dalton's law

Associated mixture rules are:

$$\begin{cases} T = T_k & : \text{mixture in thermal equilibrium} \\ V = V_k & : \text{each phase occupies the entire volume} \\ p = \sum_{k=2}^{N} p_{p\,k} & : \text{the mixture pressure is the sum of partial pressures} \\ e = \sum_{k=2}^{N} Y_k e_k & : \text{mixture internal energy definition} \end{cases}$$

The ideal gas law for a given species reads,

$$p_{p\,k} V = n_k \hat{R} T,$$

and the gas mixture pressure reads,

$$pV = \hat{R} T \sum_{k=2}^{N} n_k,$$

where $\hat{R}$ denotes the universal gas constant, in molar units. In this relation the temperature is extracted from the caloric equation of state for the mixture,

$$e = \hat{R} T \sum_{k=2}^{N} \frac{Y_k / W_k}{\gamma_k - 1},$$

where W_k denotes the molar mass and the polytropic coefficient of phase k. Consequently, the pressure reads,

$$p = \frac{\frac{e}{V} \sum_{k=2}^{N} n_k}{\sum_{k=2}^{N} \frac{Y_k/W_k}{\gamma_k - 1}} = \frac{e \sum_{k=2}^{N} \frac{n_k W_k}{V} \frac{1}{W_k}}{\sum_{k=2}^{N} \frac{Y_k/W_k}{\gamma_k - 1}},$$

finally,

$$p = \frac{\rho e \sum_{k=2}^{N} \frac{Y_k}{W_k}}{\sum_{k=2}^{N} \frac{Y_k/W_k}{\gamma_k - 1}}. \tag{2.1}$$

2.2. Each gas constituent occupies its own volume in pressure and temperature equilibrium

We now consider the opposite configuration with separated phases. Corresponding mixture rules are,

$$\begin{cases} T = T_k & : \text{mixture in thermal equilibrium} \\ v = \sum_{k=2}^{N} Y_k v_k & : \text{each phase occupies its own volume and the total volume is the sum of all sub volumes} \\ p = p_k & : \text{pressure equilibrium among the phases} \\ e = \sum_{k=2}^{N} Y_k e_k & : \text{mixture internal energy definition} \end{cases}$$

The ideal gas law for a given species now reads,

$$p_k V_k = n_k \hat{R} T,$$

In mass units it becomes,

$$p_k = \frac{n_k W_k}{V_k} \frac{\hat{R}}{W_k} T = \rho_k \frac{\hat{R}}{W_k} T.$$

Consequently the specific volume of a given phase as a function of pressure and temperature reads,

$$v_k = \frac{\hat{R}}{W_k} \frac{T}{p_k}.$$

This result is inserted in the specific volume definition,

$$v = \sum_{k=2}^{N} Y_k v_k,$$

yielding,

$$\frac{p}{T} = \rho \sum_{k=2}^{N} Y_k \frac{\hat{R}}{W_k}.$$

The mixture energy definition is now considered, resulting in the same relation as in Section 2.1:

$$e = \hat{R} T \sum_{k=2}^{N} \frac{Y_k / W_k}{\gamma_k - 1}.$$

Eliminating the temperature by combining these two relations, the following result is obtained:

$$p = \frac{\rho e \sum_{k=2}^{N} \frac{Y_k}{W_k}}{\sum_{k=2}^{N} \frac{Y_k / W_k}{\gamma_k - 1}}. \tag{2.2}$$

It is clear that both ideal mixtures models (Dalton's law Eq. (2.1) and separate phases Eq. (2.2)) merge when the fluids are ideal gases evolving in both temperature and pressure equilibrium. This remark simplifies dramatically the building of the mixture EOS. Before addressing this topic, let us present the EOS for the liquid phase and its vapor.

2.3. EOS for pure constituent

In this frame, it is assumed that each gaseous constituent ($k = 2, \dots N$) obeys the ideal gas equation of state. The EOS coefficients for the vapor (species $k = 2$) must be carefully established, in coordination with the liquid ($k = 1$) EOS, as to fit the phase diagram. The building of such EOS has been addressed in Le Métayer et al. (2004) [11], on the basis of the stiffened gas (SG) EOS. In later developments, the same authors proposed the "Noble-Abel Stiffened Gas" (NASG) [12], which improves considerably the liquid specific volume accuracy by taking into account the missing last molecular effect (repulsion) in addition to those already considered in the SG EOS (agitation and attraction). The main formulas for the NASG EOS read for a given constituent $k = 1, \dots N$ (liquid, vapor, gas),

$$\begin{cases} p_k(v_k, e_k) = (\gamma_k - 1)\dfrac{(e_k - q_k)}{v_k - b_k} - \gamma_k p_{\infty,k}, \\ T_k(p_k, v_k) = \dfrac{(v_k - b_k)\,(p_k + p_{\infty,k})}{C_{v,k}(\gamma_k - 1)}, \\ g_k(p_k, T_k) = (\gamma_k C_{v,k} - q'_k)T_k - C_{v,k}T_k \ln\left[\dfrac{T_k^{\gamma_k}}{(p_k + p_{\infty,k})^{\gamma_k - 1}}\right] + b_k p_k + q_k, \\ c_k(p_k, v_k) = v_k\sqrt{\dfrac{\gamma_k v_k\,(p_k + p_{\infty,k})}{v_k - b_k}}. \end{cases} \tag{2.3}$$

where the following parameters are needed for each phase: γ_k, $p_{\infty,k}$, $C_{v,k}$, q_k, q'_k and b_k. These parameters are constant coefficients characteristic of the thermodynamic properties of the fluid. Among them the coefficient b represents the covolume of the fluid. g_k denotes the phase k Gibbs free energy $g_k = h_k - Ts_k$ with h_k and s_k respectively the specific enthalpy and entropy. c_k denotes the phase k speed of sound.

The following results can be adapted to the SG EOS framework by setting $b_k = 0$. For all gaseous constituents ($k = 2, \dots N$), $b_k = 0$ and $p_{\infty,k} = 0$, and the above system reduces to the ideal gas EOS. *Note that, for the k-th gaseous constituent, the pressure p_k is based on the sub-volume containing the constituent. It is therefore equal to the pressure of the whole gas phase, and not to be confused with the partial pressure of the constituent in the gas phase. In the following, it is explicitly stated when a partial pressure is introduced.*

The same strategy as in [11] and [12] is repeated in order to find a formulation connecting the

saturation pressure and temperature, by equating the liquid and the vapor chemical potentials $g_1 = g_2$, leading to the following equation:

$$\ln\left(p_{sat} + p_{\infty,2}\right) = A + \frac{B + E\,p_{sat}}{T_{sat}} + C\ln\left(T_{sat}\right) + D\ln\left(p_{sat} + p_{\infty,1}\right), \tag{2.4}$$

where,

$$\begin{aligned} A &= \frac{C_{p,1} - C_{p,2} + q_2' - q_1'}{C_{p,2} - C_{v,2}}, \quad B = \frac{q_1 - q_2}{C_{p,2} - C_{v,2}}, \\ C &= \frac{C_{p,2} - C_{p,1}}{C_{p,2} - C_{v,2}}, \quad D = \frac{C_{p,1} - C_{v,1}}{C_{p,2} - C_{v,2}}, \quad E = \frac{b_1 - b_2}{C_{p,2} - C_{v,2}}. \end{aligned} \tag{2.5}$$

For liquid water and steam, the NASG fluid parameters, optimized in the [273-500K] temperature range are given in Table 1. In the same Table are given the coefficients for air[2] (in the frame of the perfect gas assumption).

Coefficients	Liquid water	Water vapor	air
C_p (J/kg/K)	4285	1401	1007
C_v (J/kg/K)	3610	955	719
γ	1.19	1.47	1.4
P_∞ (Pa)	$7028\,10^5$	0	0
q (J/kg)	-1177788	2077616	0
q' (J/kg/K)	0	14317	0
b (m^3/kg)	$6.61\,10^{-4}$	0	0
W (g/mol)	18	18	29

Table 1: Noble Abel Stiffened Gas (NASG) coefficients for water and air determined in the temperature range $[273 - 500\ K]$

These parameters are used in the computational examples of the present paper. A comparison between the NASG EOS and experimental data is displayed in Fig 1, showing good agreement.

2.4. Mixture equation of state

As presented, each constituent is addressed with the NASG EOS (reduced to the ideal gas EOS for gaseous constituents). However the mixture equation of state, based on mechanical

[2]Note that we only consider mass transfer between liquid and vapor, so the reference energy of other gaseous components is of no importance. If other mass transfers are to be considered (between gaseous components), reference energies have to be set accordingly.

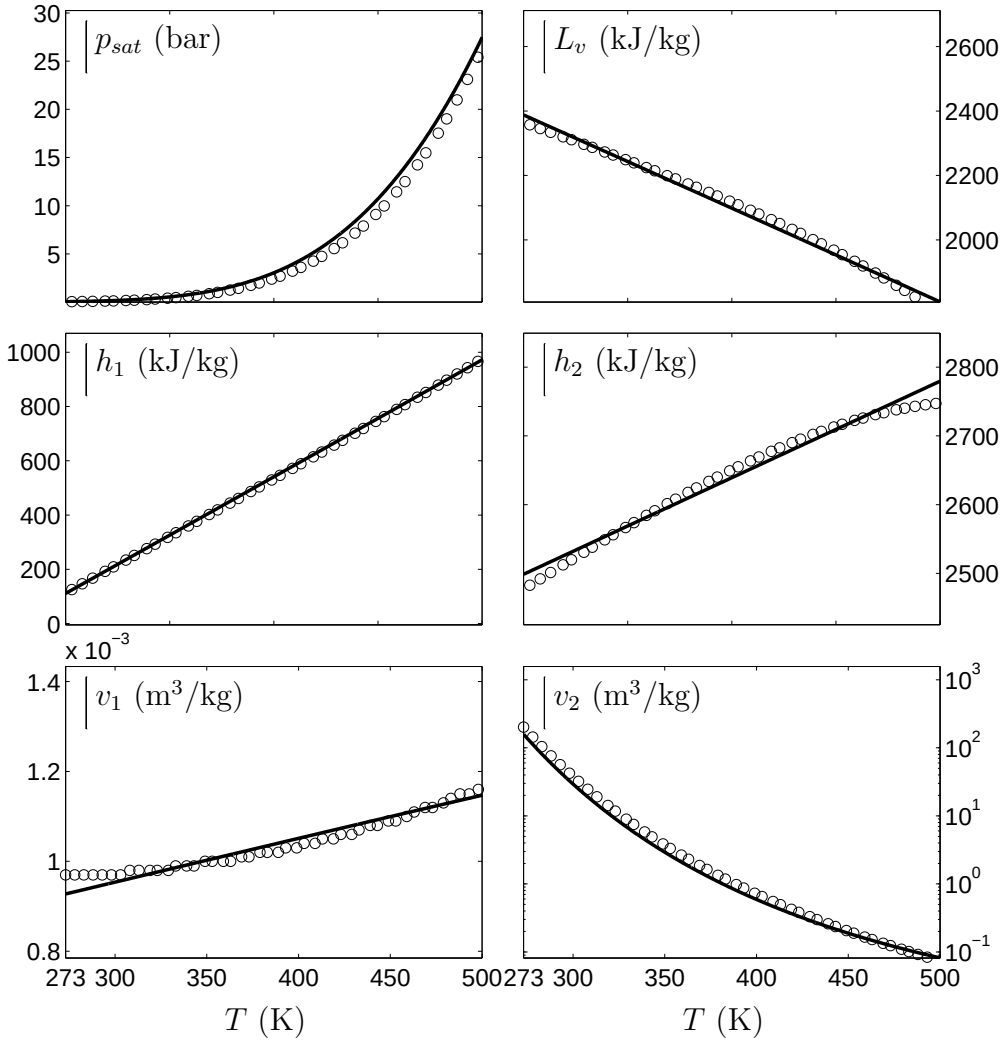

Figure 1: Comparison between experimental and theoretical saturation curves for liquid water and steam with coefficients determined in the temperature range $[273 - 500\,K]$. The symbols represent the experimental data. The thick lines represent the NASG theoretical saturation curve. P_{sat} denotes the saturation pressure, L_v the latent heat, h the specific enthalpy and v the specific volume.

and thermal equilibrium has yet to be built. Under the assumption of mechanical and thermal equilibrium, an inherent assumption to the 4-equation model, we have:

$$\begin{cases} T = T_k \quad \forall k, \\ p = p_k \quad \forall k, \\ v = \sum_{k=1}^{N} (Y_k v_k), \\ e = \sum_{k=1}^{N} (Y_k e_k). \end{cases} \tag{2.6}$$

with v the mixture specific volume.

As shown at the beginning of this Section, considering (2.6) for the mixture of gases is equivalent to Dalton's law. Therefore the computed mixture pressure for the gas mixture will be in agreement with both Dalton's law in the gas mixture and with the liquid-gas interface condition of equal pressures. System (2.6) summarizes consequently correctly the separate phase mixture model between the liquid and the gas mixture on one hand and the ideal gas mixture on the other hand.

From the expressions given in Eqs. (2.3) for pure constituents, the specific volumes and internal energies can be expressed as:

$$\begin{cases} v_k(p_k, T_k) = \dfrac{(\gamma_k - 1) C_{v,k} T_k}{p_k + p_{\infty,k}} + b_k \\ e_k(p_k, T_k) = \dfrac{p_k + \gamma_k p_{\infty,k}}{p_k + p_{\infty,k}} C_{v,k} T_k + q_k, \end{cases} \tag{2.7}$$

which can be rewritten to give two expressions of the temperature (since $T_k = T, \forall k$):

$$T = \frac{v - \sum_{k=1}^{N} Y_k b_k}{\sum_{k=1}^{N} \frac{Y_k (\gamma_k - 1) C_{v,k}}{p + p_{\infty,k}}}, \tag{2.8}$$

$$T = \frac{e - \sum_{k=1}^{N} Y_k q_k}{\sum_{k=1}^{N} Y_k C_{v,k} \left(\frac{p + \gamma_k p_{\infty,k}}{p + p_{\infty,k}} \right)}. \tag{2.9}$$

Equating these two expressions, and taking into account that $p_{\infty,k} = b_k = 0, \forall k > 1$, a quadratic expression for the mixture pressure is obtained as:

$$p = \frac{b + \sqrt{b^2 + 4ac}}{2a}, \tag{2.10}$$

with:

$$\begin{cases} a = \bar{C}_v, \\ b = \left(\dfrac{e-\bar{q}}{v-\bar{b}}\right)\left(\bar{C}_p - \bar{C}_v\right) - p_{\infty,1}\bar{C}_v - p_{\infty,1}Y_1\left(C_{p,1} - C_{v,1}\right), \\ c = \left(\dfrac{e-\bar{q}}{v-\bar{b}}\right)p_{\infty 1}\left[\bar{C}_p - \bar{C}_v - Y_1\left(C_{p,1} - C_{v,1}\right)\right], \end{cases} \tag{2.11}$$

where mixture quantities are introduced:

$$\bar{C}_v = \sum_{k=1}^{N} Y_k C_{v,k}, \quad \bar{C}_p = \sum_{k=1}^{N} Y_k C_{p,k}, \quad \bar{q} = \sum_{k=1}^{N} Y_k q_k, \quad \bar{b} = \sum_{k=1}^{N} Y_k b_k. \tag{2.12}$$

Note that, for $Y_1 = 0$ (no liquid), the above equation reduces to

$$p = \left(\frac{e-\bar{q}}{v}\right)\frac{(\bar{C}_p - \bar{C}_v)}{\bar{C}_v},$$

which after substituting $e = \sum_{k=2}^{N} e_k$, and noticing that $(\bar{C}_p - \bar{C}_v) = \sum_{k=2}^{N} Y_k R/W_k$, leads to:

$$p = \sum_{k=2}^{N} Y_k \rho R T/W_k,$$

or, in other words, the classical law of Dalton for the gas mixture. This provides an additional verification as to the possibility of considering each gas constituent to be in its own volume, as discussed in the flow model section. Albeit the apparent simplicity of the thermodynamic closure chosen, the phase transition model presented here may be extended to other thermodynamic closures given each phase EOS is convex.

3. Phase transition model

3.1. Objective

When phase transition is addressed between the liquid and its vapor, only the first two constituents conservation equations are modified as:

$$\begin{cases} \dfrac{\partial \rho Y_1}{\partial t} + div(\rho Y_1 \mathbf{u}) &= \rho\nu(g_2 - g_1) \\ \dfrac{\partial \rho Y_2}{\partial t} + div(\rho Y_2 \mathbf{u}) &= -\rho\nu(g_2 - g_1) \end{cases} \tag{3.1}$$

where g_k denotes the phase k Gibbs free energy $g_k = h_k - T s_k$ with h_k and s_k respectively the specific enthalpy and entropy . $\nu(A_I, T, p)$ represents a relaxation parameter that controls the

rate at which thermodynamic equilibrium is reached. It is a function of the specific interfacial area A_I, temperature and pressure. Its determination is possible only when the interfacial area A_I is available, as with droplets and bubbly flows (see Furfaro and Saurel, (2016) for example [13]) and sometimes for stratified flows. A natural way to determine this exchange area would be to use a very high resolution mesh to capture interfaces at all spatial scales. However this strategy would require tremendous computing resources and can hardly be envisaged when considering large-sized problems. Nevertheless a realistic method in specific limit situations is to consider instantaneous thermodynamical relaxation between phases by the use of additional source terms [9]. In the present work, ν is considered very large, so that relaxation to thermodynamic equilibrium is immediate.

During the phase transition process, the mixture specific volume $v = 1/\rho$ and energy e do not vary. The mass fractions for all gaseous species other than the vapor ($Y_{k\geq 3}$) also remain constant. However, pressure and temperature do vary, reaching their equilibrium values (p^*, T^*). The phase transition model thus reduces to computing the equilibrium state (p^*, T^*, Y_k^*), at every time step, from the state described by (p, T, v, e, Y_k).

Since pressure and temperature are functions of (v, e, Y_k), and v and e are constant during the phase transition, the primary goal of the procedure is to compute accurately Y_1^*, since Y_2^* is linked through mass conservation:

$$Y_2^* = 1 - Y_1^* - \sum_{k\geq 3} Y_k.$$

In our approach, phase transition is decoupled of transport and wave propagation using a fractional step method, essentially reducing the model to setting $Y_1 = Y_1^*$ and $Y_2 = Y_2^*$ after each hyperbolic step.

3.2. Expression of the thermo-chemical equilibrium

When only liquid and vapor are present ($Y_{k\geq 3} = 0$), as in our previous paper, the thermo-chemical equilibrium directly translates into $p^* = p_{sat}(T^*)$, independently of Y_1^*. Here a consequent complexity is added, as the thermo-chemical equilibrium translates to the vapor *partial* pressure in the gas phase being equal to the saturation pressure at the current temperature.

The relation between p^* and T^* then depends on the composition of the multicomponent gas $Y_{k\geq 2}$. Within ideal gas mixtures , the vapor partial pressure is directly proportional to the vapor molar fraction:

$$p_{partial} = \frac{Y_2/W_2}{\sum_{k\geq 2} Y_k/W_k}.p, \tag{3.2}$$

so that the expression satisfied at thermochemical equilibrium is

$$p_{sat}(T^*) = p_{partial} = \frac{Y_2^*/W_2}{\sum_{k\geq 2} Y_k^*/W_k}.p^*. \tag{3.3}$$

This relation is indeed essential in that it allows an equilibrium of liquid and multicomponent gas in conditions below saturation (for instance water condensation at ambient temperature and pressure).

3.3. Solution of a simplified problem

Instead of solving the thermochemical equilibrium at constant $v^* = v$, $e^* = e$ and $Y^*_{k\geq 3} = Y_{k\geq 3}$, and computing (p^*, T^*, Y_1^*) (our method's goal) , let us assume $p^* = p$, $T^* = T$ and $Y^*_{k\geq 3} = Y_{k\geq 3}$ are constant, and v and e are varying. The thermochemical equilibrium problem is then straightforward to solve analytically:

Case 1 $T > T_{sat}(p)$: the mixture is necessarily purely gaseous. We then have $Y_1^* = 0$.

Case 2 $T < T_{sat}(p)$: the mixture can be purely gaseous when the vapor quantity does not exceed its saturation limit, to be established hereafter. If this value is reached, then liquid is present.

The attainable limit for the vapor mass fraction before condensation in the multi-component gas is obtained by solving $p_{partial} = p_{sat}(T)$. Using Eq. (3.2), one gets

$$Y_2^{sat} = \frac{p_{sat}(T)W_2}{p - p_{sat}(T)} \sum_{k\geq 3} Y_k/W_k \tag{3.4}$$

Below the saturation temperature, we then have

$$Y_2^* = \min\left(Y_2^{sat}, 1 - \sum_{k\geq 3} Y_k\right). \tag{3.5}$$

The equilibrium mass fraction Y_2^* cannot exceed the available room $(1 - \sum_{k\geq 3} Y_k)$, nor can it exceed the saturation limit, after which liquid is present. Y_1^* is then deduced from mass conservation. Figure 2 shows the solution for Y_1^* and Y_2^* of this simple problem, for a mixture of liquid water, water vapor and air ($N = 3$), at atmospheric pressure, and a mixture temperature of 350K. On the right handside of the plot, there is so much air content that water vapor is diluted enough (below the saturation limit), and no liquid is present. On the left part, Y_2^* varies linearly with Y_3, as a consequence of the saturation relation $p_{partial} = p_{sat}(T)$. The Figure also indicates the variation of the mixture specific volume, which increases up to the saturation limit (since the liquid fraction diminishes), and then decreases, because air is heavier than water vapor.

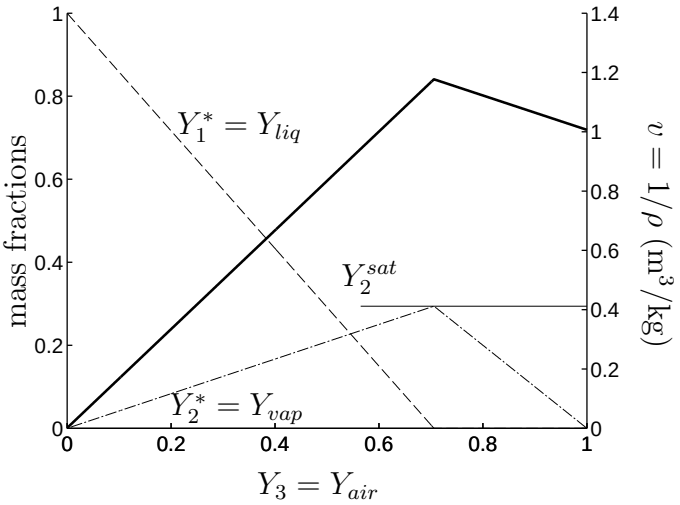

Figure 2: Equilibrium mass fractions obtained from water liquid/vapor, as a function of the air mass fraction. Conditions: atmospheric pressure, T=350K. dashed line: Y_1^*, dashed-dotted: Y_2^*. The thick line represents the specific volume obtained for the mixture in these conditions.

This simplified problem is convenient for two reasons: it illustrates well the problem to be solved, and also provides a simple way to compute initial or boundary conditions in a simulation, compatible of the thermodynamic equilibrium solver.

When the problem is to be solved at constant (v, e), instead of (p, T), an analytic approach is no longer possible, and the problem has to be solved numerically. In the following section, we present an alternative to a tedious iterative process.

4. Thermochemical relaxation algorithm

The idea of our method is to gradually reach the exact solution (typically in 1 to 3 time steps of the flow solver), by providing a fair approximation for Y_1^*, where iterative approaches, such as the one promoted in Le Metayer et al. (2013) [9], directly computes the exact solution. In that direction, we will follow a similar strategy than in our previous work [1], extended to the fact that the relation between pressure and saturation pressure is modified (3.3), and now depends on the result (since the partial pressure is a function of Y_2). First, let us bound the result for Y_1^* and Y_2^*:

$$\begin{cases} Y_{min} = \epsilon, \\ Y_{max} = 1 - Y_{min} - \sum_{k=3}^{N} Y_k. \end{cases} \tag{4.1}$$

With $\epsilon \to 0$ for numerical purposes, typically on the order of 10^{-8}. As in our previous work [1], we first assume $Y_1^* = Y_{min}$, to check if the system has a solution without liquid. Under this assumption, pressure and temperature are computed by use of the mixture equation of state (2.8) and (2.10):

$$\begin{cases} p = \quad p(v, e, Y), \\ T = \quad T(v, e, Y), \end{cases}$$

since the mixture variables v and e are invariant through phase transition. Additionally, we compute the corresponding partial pressure for vapor Eq. (3.2), and compare it to the saturation pressure (2.4). If the partial pressure is below the saturation pressure, no liquid is present and the solution is $Y_1^* = Y_{min}$ and $Y_2^* = Y_{max}$. Note that, unlike in our last contribution, there is no need to check the existence of the pure liquid phase: no matter how small ϵ is chosen , there will always be a (very small) solution for Y_2^* satisfying that its partial pressure is equal to the saturation pressure. This aspect is commented in Sec. 5, about the algorithm's stability. If

$Y_1^* \neq Y_{min}$, the following system has to be solved

$$\begin{cases} p_{partial} = x_v^*.p^* = p_{sat}(T^*), \\ v = Y_1^* v_1(T^*, p^*) + Y_2^* v_2(T^*, p^*) + \sum_{k=3}^N Y_k v_k(T^*, p^*), \\ e = Y_1^* e_1(T^*, p^*) + Y_2^* e_2(T^*, p^*) + \sum_{k=3}^N Y_k e_k(T^*, p^*), \end{cases} \tag{4.2}$$

leaving us with three equations for three unknowns (p^*, T^*, Y_1^*). The vapor molar fraction x_v^* is defined as,

$$x_v^* = \frac{Y_2^*/W_2}{Y_2^*/W_2 + \sum_{k=3}^N Y_k/W_k}, \tag{4.3}$$

We will now evaluate three approximate expressions for Y_1^*. Rewriting the specific volume definition from System (4.2) leads to the following approximate expression:

$$Y_1^m(p,T) = \frac{v - v_g(p,T)}{v_1(p,T) - v_2(p,T)}, \qquad \text{with} \qquad v_g(p,T) = \left(1 - \sum_{k=3}^N Y_k\right) v_2(p,T) + \sum_{k=3}^N Y_k v_k(p,T). \tag{4.4}$$

Any mass fraction computed from this formula after the hyperbolic step will satisfy the mass conservation $\forall (p,T)$. Similarly, we can rewrite the specific mixture energy definition from System (4.2):

$$Y_1^e(p,T) = \frac{e - e_g(p,T)}{e_1(p,T) - e_2(p,T)}, \qquad \text{with} \qquad e_g(p,T) = \left(1 - \sum_{k=3}^N Y_k\right) e_2(p,T) + \sum_{k=3}^N Y_k e_k(p,T). \tag{4.5}$$

Equations for $Y_2^m(p,T)$ and $Y_2^e(p,T)$ (expressed for the vapor phase instead of the liquid phase) can be obtained as

$$Y_2 = 1 - Y_1 - \sum_{k=3}^N Y_k.$$

In our previous work [1], these two functions of (p,T) could be reduced to functions of p in finding the equilibrium as $p = p_{sat}(T)$ for a liquid-vapor mixture. As shown in Eq. (3.3), the new relation $p_{partial} = p_{sat}(T^*)$ includes an additional dependence on Y_2^* (or, equivalently, on

Y_1^*), leading to Eq. (3.3), reminded here:

$$Y_2^{sat}(p,T) = \frac{p_{sat}(T)W_2}{p - p_{sat}(T)} \sum_{k\geq 3} Y_k/W_k. \tag{4.6}$$

The exact solution to the problem is found in pressure and temperature conditions satisfying all three Eqs. of (4.2), or, equivalently:

$$Y_2^m(p^*,T^*) = Y_2^e(p^*,T^*) = Y_2^{sat}(p^*,T^*).$$

This is illustrated in Fig. 3, for a set of conditions initially out of equilibrium (30K below saturation).
In this graph,

- the light gray surface represents the mass conservation condition: $Y_2^m(p,T)$,
- the medium gray surface represents the energy conservation condition: $Y_2^e(p,T)$,
- the dark gray surface, represents the thermo-chemical equilibrium condition: $Y_2^{sat}(p,T)$.

The algorithm consists in computing three approximations for Y_2^*:

- $Y^m = Y_2^m(p,T)$ is evaluated for the initial values of (p,x_v) (from the hyperbolic step), and $T = T_{sat}(x_v.p)$,
- $Y^e = Y_2^e(p,T)$ is evaluated for the initial values of (p,x_v) (from the hyperbolic step), and $T = T_{sat}(x_v.p)$,
- $Y^{sat} = Y_2^{sat}(p,T)$ is evaluated at the initial (p,T).

As in [1], the idea of this model is then to pick the closest value to the initial value, under the condition that all three associated mass transfers are of the same sign. This idea is reminiscent of the well known Minmod slope limiter widely used in higher order CFD solvers for gradients limitation. In other words, we introduce:

$$\begin{cases} r_1 = (Y^m - Y_2)\,(Y^e - Y_2)\,, \\ r_2 = (Y^m - Y_2)\,(Y^{sat} - Y_2)\,, \end{cases} \tag{4.7}$$

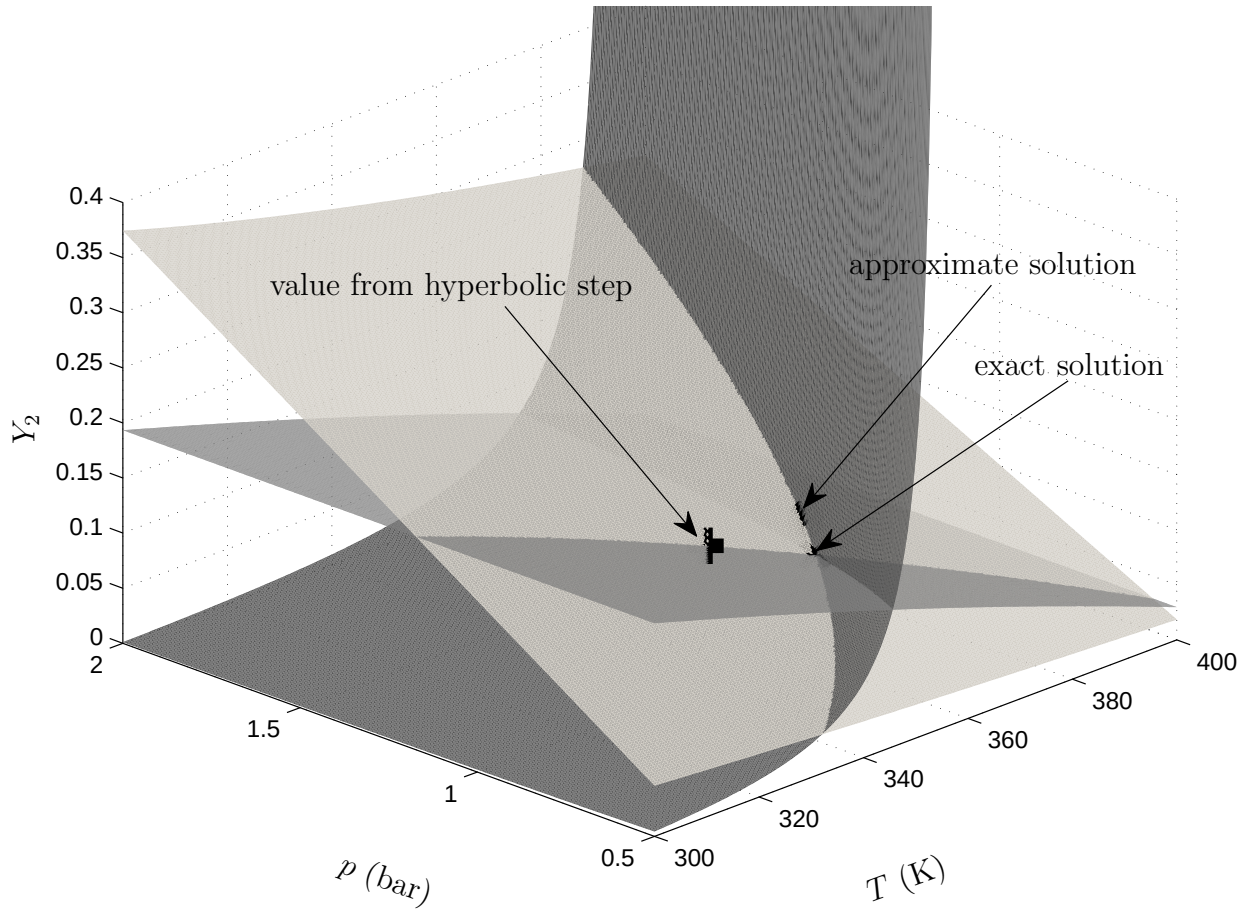

Figure 3: Illustration of the algorithm for the multicomponent phase transition solver. From light gray to dark gray: $Y^m(p^*, T^*), Y^e(p^*, T^*), Y^{sat}(p^*, T^*)$. The exact solution of the problem is found at the intersection of the three surfaces. The value from hyperbolic step corresponds to the initial conditions of the algorithm: $Y_2 = 2.Y_2^*$ (far from equilibrium) at $p = 1$atm, $T = T_{sat}(p) - 30K = 343K$, and $Y_3 = 0.1$. Here, computations lead to $Y_2^* = 0.1$, $Y^m = 0.11$, $Y^e = 0.9$, $Y^{sat} = 0.03$, so that the algorithm retains Y^m, within 10% of the exact solution.

where Y_2 is the initial mass fraction (from the hyperbolic step), and Y^m, Y^e, Y^{sat} are three estimates for the equilibrium Y_2^*.

- If $r_1 < 0$, or $r_2 < 0$, no mass transfer happens: $Y_2^* = Y_2$
- Else, the minimum mass transfer is applied. For instance, if Y^m is closest to Y_2 (out of Y^m, Y^e, Y^{sat}), then $Y_2^* = Y^m$.

Under the latter condition, this can be implemented as:

$$Y_2^* = Y_2 + sgn\left[Y^m - Y_2\right] \times Min\left[|Y^m - Y_2|, |Y^e - Y_2|, |Y^{sat} - Y_2|\right] \tag{4.8}$$

Summary of the procedure:

1) Search for a solution without liquid

- The limit case $Y_l^* \to \epsilon$ is considered with computation of the pressure and temperature according to the mixture equation of state (2.8) and (2.10). Additionally the corresponding saturation pressure and partial pressure for vapor are computed according to Eqs. (2.4) and (3.2).
- If the partial pressure is below the saturation pressure, no liquid is to be considered and the solution is $Y_1^* = Y_{min}$ and $Y_2 = Y_{max}$ according to Eq. (4.1).

2) If liquid is present, the thermodynamic equilibrium is to be computed

- Computation of the liquid mass fraction at equilibrium Y_1^* according to the Minmod-like procedure Eq. (4.8) using Eqs. Y^m (4.4), Y^e (4.5), Y^{sat} (4.6), (4.7), and the EOS (2.7).

5. Algorithm stability

In a previous contribution [1] in which only liquid and vapor were considered, a major challenge was to deal with the pure liquid limit. Let us consider pure liquid water, initially at 300K and 1atm. If a small quantity ϵ of vapor appears, the system has to go to thermochemical equilibrium, no matter how far off the initial conditions are. Because of the high heat capacity and low compressibility of the water, the process is mostly isothermal, and important pressure fluctuations could be observed. This motivated the introduction of a correction on the pressure

used to estimate Y^m and Y^e, in order to improve the model capabilities of dealing with the transition from pure liquid to two-phase mixture in the limit $Y_{k\geq 2} \to 0$.

Here, there is no need for such correction. The situation detailed above, in which a mixture can be found very far off equilibrium after the hyperbolic step, can not be encountered. In the present work's context, we can find a value for the vapor mass fraction $Y_2 = Y_{vap}$, no matter the conditions given, as traces of incondensable gas are present $Y_3 = Y_{air}$. At 300K and 1atm for a mixture of liquid water , vapor water and air, assuming $Y_3 = \epsilon$ (which can be as small as numerically allowed) will lead to a very small but non zero Y_2. With these considerations, the lack of continuity in the transition from pure liquid to two-phase mixture, present in the liquid-vapor model, simply vanish in this new context.

Additionally, let us note that presence of air in water is physical (dissolved), and can be estimated through Henry's law. For instance, in ambient conditions, the air mass fraction dissolved is of order $Y_3 = 10^{-5}$, leading to a value of Y_2 of the same order, satisfying the system (4.2). Indeed, such low values do not have significant effect on mean density and energy, which remain close to the pure phase values.

In practical computations presented in this paper, unless stated otherwise, a small value is set for Y_3 in liquid, and Y_2 is computed accordingly, following Eq. (3.5) for the initial prescribed pressure and temperature. Another important aspect in the algorithm's stability is that $\forall(p,T)$ (a priori away from the equilibrium point), one of the three functions $Y_2^m(p,T), Y_2^e(p,T), Y_2^{sat}(p,T)$ is above (or below) the exact solution for Y_2^*. This is clearly visible in Fig. 3. Although we have not proved this result because of the non-linear dependence of $p_{sat}(T)$ (as in our previous contribution), we have not found a case in which this does not apply. As a consequence:

- If $Y_2 > Y_2^*$, mass transfer will be applied only if Y^m, Y^e, Y^{sat} are less than Y_2 (they cannot be all Y_2 at the same time given the above property), and one of them at least is superior to Y_2^*. The algorithm then cannot "overestimate" the mass transfer.

- The same thing can be said when $Y_2 < Y_2^*$.

- Last but not least, since $0 < Y_2 < 1 - \sum_{k\geq 3} Y_k$ (given the hyperbolic step is properly implemented), and the exact solution also satisfies $0 < Y_2 < 1 - \sum_{k\geq 3} Y_k$, the approximate

solution from the algorithm can never go out of bound.

6. Numerical results

The robustness and accuracy of the present thermochemical relaxation algorithm have been proven in a previous contribution [1] for two-phase flows containing a liquid and its own vapor only. In the present context, non-condensable gases must be dealt with. The developed present relaxation solver is to be compared with an iterative algorithm such as the one promoted in Le Metayer et al. (2013) [9]. Unlike this last algorithm, the notion of vapor molar fraction and partial pressures in the gas phase must be taken into account, bringing additional difficulties. The corresponding iterative solver is consequently recalled and modified in Appendix.

To illustrate robustness and accuracy of the relaxation algorithm, a shock tube containing liquid water, its own vapor and some non-condensable air is considered, with variable initial conditions. Shock tube tests appear as excellent benchmarks as the flow contains shock waves, contact discontinuities and rarefaction fans that create some arduous conditions. In this section, the tube is 1 meter long and the initial discontinuity is located at 0.5 meter. Boundary conditions are non-reflecting. The computations that follow are addressed with the MUSCL Hancock method using VanLeer's slope limiter and the HLLC Riemann solver (see Toro (1997) [14], Saurel et al. (2016) [6], for details). This section compares the results obtained with the present relaxation solver and the classic root-finding procedure method given in Appendix. Unless stated otherwise, the one-dimensional simulations are computations are addressed on meshes with 100 cells.

6.1. Shock tube test with a mixture far from the phase bounds

A two-phase mixture with initial mass fractions set at $Y_1 = 0.1$ (liquid), $Y_2 = 0.2$ (vapor) and $Y_3 = 0.7$ (air) is considered throughout the entire tube with an initial pressure ratio of 2, resulting in the presence of initial density and temperature discontinuities. The results are shown at time $t \approx 1$ms in Fig. 4.

Perfect agreement is obtained between the present relaxation solver and the non-linear iterative method. Clearly the shock compression yields evaporation and the rarefaction results into condensation.

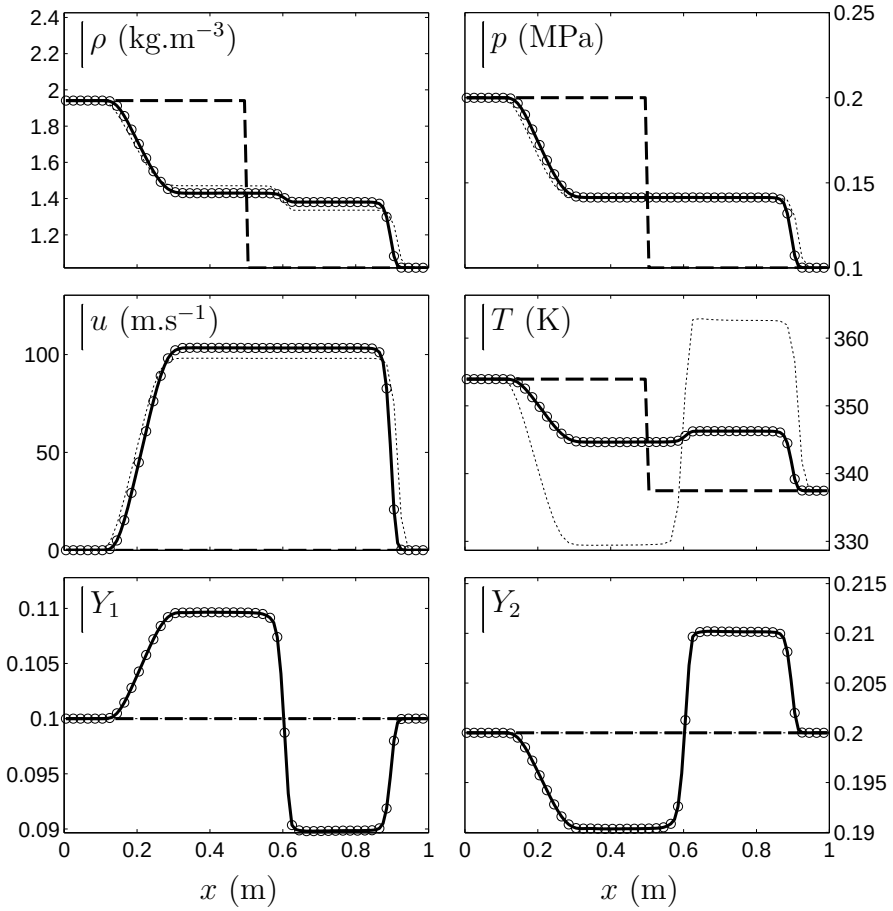

Figure 4: Comparison of the present relaxation algorithm (thick lines) versus the non-linear iterative solver (symbols). Shock tube test with a two-phase mixture made of liquid water, vapor water and air. The dotted lines represent the solutions without phase transition. The dashed lines represent the initial conditions: $p_l = 2{\cdot}10^5$ Pa, $p_r = 10^5$Pa, $u_l = u_r = 0$m.s^{-1}, $Y_1^{left} = Y_1^{right} = 0.1$, $Y_2^{left} = Y_2^{right} = 0.2$ and $Y_3^{left} = Y_3^{right} = 0.7$. Final time: $t \approx 1$ms. Mesh: 100 cells. For the sake of visualization, only 50 symbols out of 100 are plotted for the iterative method.

6.2. Shock tube test with with a mixture with air in major proportions

In the direction of natural or industrial flows, let us now consider tests with imposed pressure, temperature and air mass fractions initially. The proportion of liquid and vapor are then deduced according to Eq. (3.5). The following test considers a shock tube with an initial pressure ratio of 2 and an initial temperature of $T = 293$K throughout the tube. The air mass fraction is initially set at $Y_3 = 0.98$ in the whole tube. The liquid and vapor mass fractions are then deduced as $Y_1 \simeq 1.073 \cdot 10^{-2}$ and $Y_2 \simeq 9.263 \cdot 10^{-3}$ in the left chamber and $Y_1 \simeq 1.186 \cdot 10^{-3}$ and $Y_2 \simeq 1.881 \cdot 10^{-2}$ in the right chamber. The results are shown at time $t \approx 1$ms in Fig. 5.

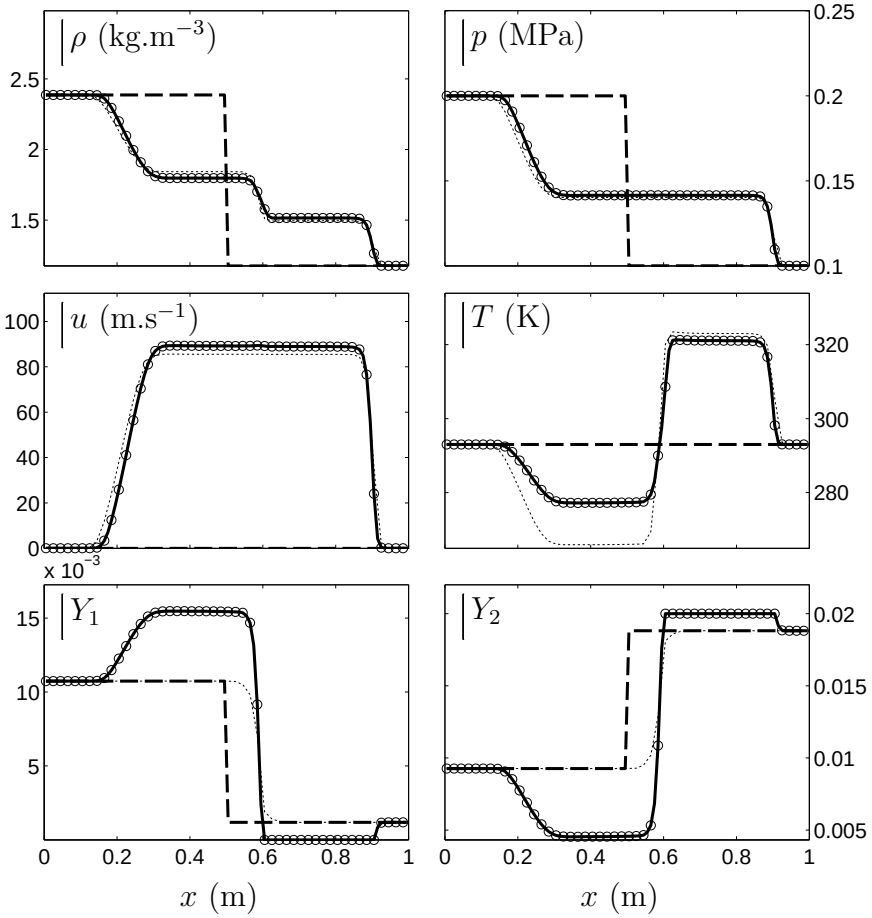

Figure 5: Comparison of the present relaxation algorithm (thick lines) versus the non-linear iterative solver (symbols). Shock tube test with a two-phase mixture with air in major proportions. The dotted lines represent the solutions without phase transition. The dashed lines represent the initial conditions: $p_l = 2 \cdot 10^5$ Pa, $p_r = 10^5$Pa, $u_l = u_r = 0$m.s^{-1}, $Y_1^{left} \simeq 1.073 \cdot 10^{-2}$, $Y_1^{right} \simeq 1.186 \cdot 10^{-3}$, $Y_2^{left} = \simeq 9.263 \cdot 10^{-3}$, $Y_2^{right} = \simeq 1.881 \cdot 10^{-2}$ and $Y_3^{left} = Y_3^{right} = 0.98$. Final time: $t \approx 1$ms. Mesh: 100 cells. For the sake of visualization, only 50 symbols out of 100 are plotted for the iterative method.

Perfect agreement is obtained between the two solvers. The shock compression results in total evaporation of the liquid water and the rarefaction results in condensation. Disappearance of liquid water is computed without oscillations by the two methods.

6.3. Shock tube test with with a mixture near pure mainly made of water

The previous mass fractions are reversed by considering $Y_3 = 10^{-5}$ and $T = 293$K initially throughout the tube, corresponding to a subcooled liquid. The following test considers a shock tube with an initial pressure ratio of 2. The liquid and vapor mass fractions are then deduced as $Y_1 \simeq 0.9999899$ and $Y_2 \simeq 9.426 \cdot 10^{-8}$ in the left chamber and $Y_1 \simeq 0.99989$ and $Y_2 \simeq 1.919 \cdot 10^{-7}$ in the right chamber. The results are shown at time $t \approx 1.5$ms in Fig. 6.

Perfect agreement is again obtained between the two solvers. The liquid phase having the highest internal heat capacity, the resulting flow is quasi-isothermal despite the slight evaporation and condensation processes appearing through the shock and rarefaction.

6.4. Double expansion test with a two-phase mixture mainly made of liquid water

The following test mimics cavitation in an initial subcooled liquid. The initial pressure, temperature and air mass fractions are respectively 1bar, $T = 293$K and $Y_3 = 10^{-5}$ throughout the entire tube. The liquid and vapor mass fractions are then deduced as $Y_1 \simeq 0.99989$ and $Y_2 \simeq 1.919 \cdot 10^{-7}$ in the left and right chambers. The initial velocity is set at -1m.s^{-1} at left and -1m.s^{-1} at right. The results are shown at time $t \approx 3.5$ms in Fig. 7.

Perfect agreement is again obtained between the two solvers. Appearance of vapor in the liquid is computed without oscillations by the two methods.

7. Computational time, efficiency and simplicity

All computational examples considered in this paper led to the same observation: the present relaxation solver is much faster than the root-finding iterative algorithm. The time gain is about 50%. The main argument for this time gain is related to its simplicity: the relaxation solver presents a straight-forward implementation whereas the iterative method requires solving a non-linear-algebraic model that may cause difficulties as a result of non-linearities. Besides, the root-finding iterative method requires the calculation of the saturation pressure via Eq. (2.4)

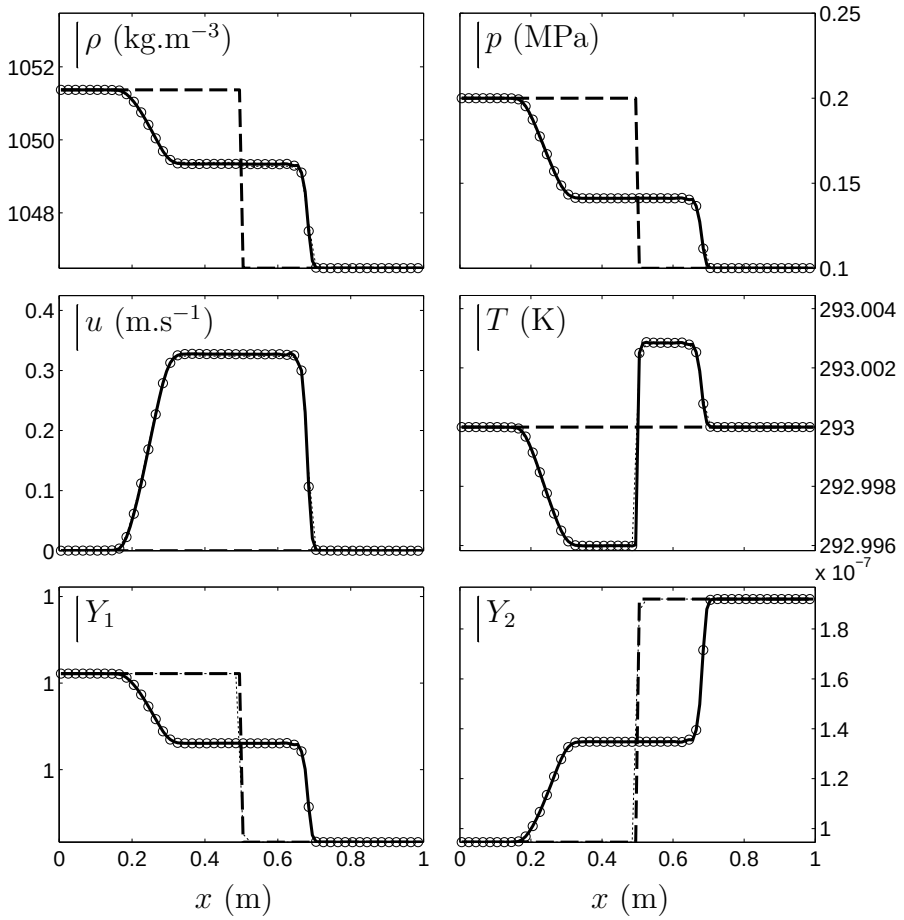

Figure 6: Comparison of the present relaxation algorithm (thick lines) versus the non-linear iterative solver (symbols). Shock tube test with a two-phase mixture mainly made of liquid water. The dotted lines represent the solutions without phase transition. The dashed lines represent the initial conditions: $p_l = 2 \cdot 10^5$ Pa, $p_r = 10^5$Pa, $u_l = u_r = 0$m.s^{-1}, $Y_1^{left} \simeq 0.9999899$, $Y_1^{right} \simeq 0.99989$, $Y_2^{left} \simeq 9.45 \cdot 10^{-8}$, $Y_2^{right} \simeq 1.919 \cdot 10^{-7}$ and $Y_3^{left} = Y_3^{right} = 10^{-5}$. Final time: $t \approx 1.5$ms. Mesh: 100 cells. For the sake of visualization, only 50 symbols out of 100 are plotted for the iterative method.

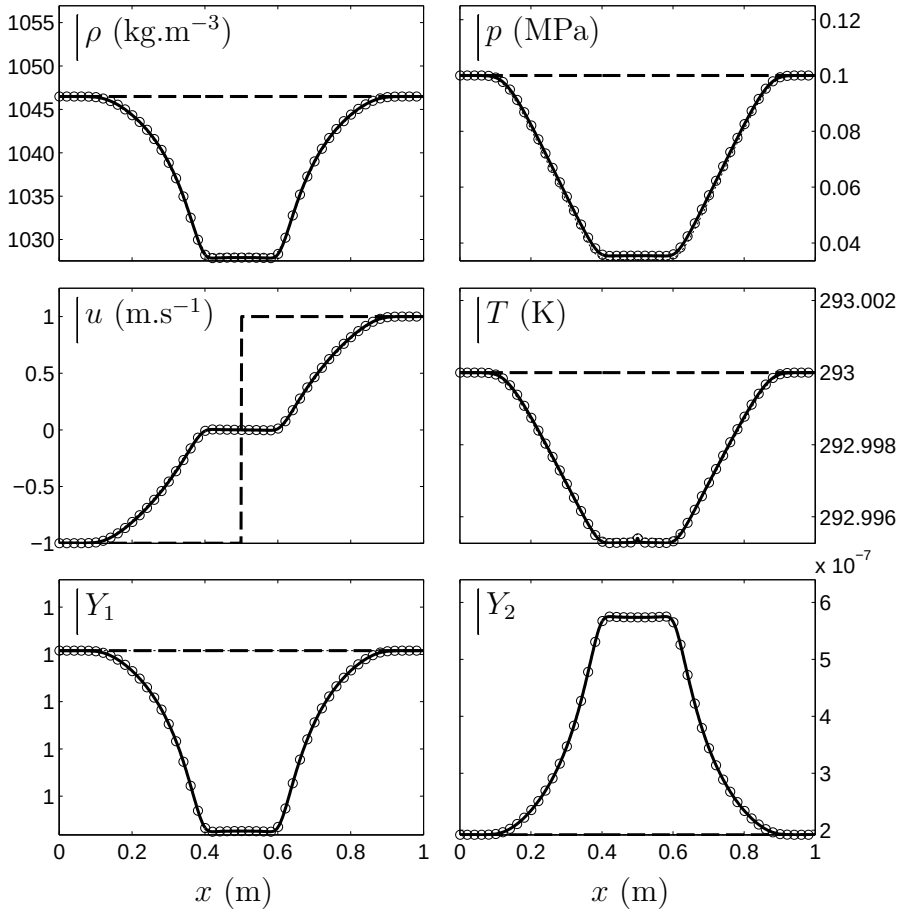

Figure 7: Comparison of the present relaxation algorithm (thick lines) versus the non-linear iterative solver (symbols). Double expansion test with a mixture mainly made of liquid water. The dotted lines represent the solutions without phase transition. The dashed lines represent the initial conditions: $p_l = 2 \cdot 10^5$ Pa, $p_r = 10^5$Pa, $u_l = -1$m.s^{-1}, $u_r = 1$m.s^{-1}, $Y_1^{left} = Y_1^{right} \simeq 0.99989$, $Y_2^{right} = Y_2^{right} \simeq 1.919 \cdot 10^{-7}$ and $Y_l^{air} = Y_r^{air} = 10^{-4}$. Final time: $t \approx 3.5$ms. Mesh: 100 cells. For the sake of visualization, only 50 symbols out of 100 are plotted for the iterative method.

at each iterative step, which itself requires an iterative method. The robustness of the present method is quite independent of the mesh resolution or the order of accuracy of the numerical scheme. For instance, Fig 8 repeats the test case already presented in Fig 5, with a 10-cell mesh and first order Godunov numerical scheme. These results are very reasonable, proving robustness of the method. Results for the same test case are also given in Fig 8 for a higher-order solver (MUSCL-Hancock scheme with the Superbee limiter), on a 1000-cell mesh. Again, perfect agreement is found between the present relaxation solver and the non-linear iterative method.

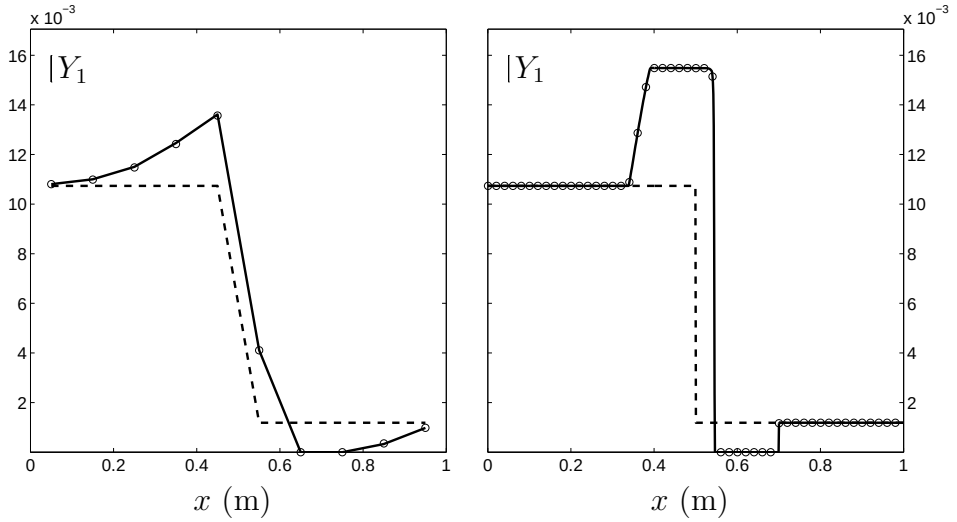

Figure 8: Comparison of the present relaxation algorithm (thick lines) versus the non-linear iterative solver (symbols). Shock tube test with a two-phase mixture mainly made of air, computed on coarse (left figure) and a fine (right figure) meshes to assess method robustness. The dashed lines represent the initial conditions: $p_l = 2 \cdot 10^5$ Pa, $p_r = 10^5$Pa, $u_l = u_r = 0\text{m.s}^{-1}$, $Y_1^{left} \simeq 1.073 \cdot 10^{-2}$, $Y_1^{right} \simeq 1.186 \cdot 10^{-3}$, $Y_2^{left} =\simeq 9.263 \cdot 10^{-3}$, $Y_2^{right} =\simeq 1.881 \cdot 10^{-2}$ and $Y_3^{left} = Y_3^{right} = 0.98$. Final time: $t \approx 0.5$ms. The figure on the left represents the solutions with a 10-cell mesh and first order Godunov numerical scheme. The figure on the right represents the solutions with a 1000-cell mesh and MUSCL-Hancock scheme with Superbee limiter. For the sake of visualization, only 50 symbols out of 1000 are plotted for the iterative method in the figure on the right. The relaxation method and iterative one tend to the same solution even with the coarse mesh.

8. Multi-dimensional illustrations

8.1. Evaporating liquid jet

In this section, the capabilities of the flow model are illustrated on an evaporating liquid jet configuration in conditions typical of cryotechnic rocket engines during the ignition phase (for

which the engine has not yet reached supercritical conditions). The flow consists of a coaxial liquid oxygen jet surrounded by a high-speed hydrogen flow, injected in conditions above the saturation point of the inner oxygen core, which then evaporates whilst being destabilized. Such a case is very challenging, because there is initially no vapor oxygen, and the phase transfer model developed is the only possible term for vapor production. The stiffened gas EOS is used, the parameters for oxygen and hydrogen are given in Table 2. The 2D computations are carried

Coefficients	Liquid phase (O_2)	Vapor phase (O_2)	Hydrogen (H_2)
C_p (J/kg/K)	1702	780	14256
C_v (J/kg/K)	695	531	10183
γ	2.45	1.47	1.4
P_∞ (bar)	1062	0	0
q (J/kg)	-258000	6900	$-1.2.10^6$
q' (J/kg/K)	0	-9280	0

Table 2: Stiffened gas coefficients for the simulation of the evaporating liquid jet.

out on a simplified geometry given in Fig. 9.

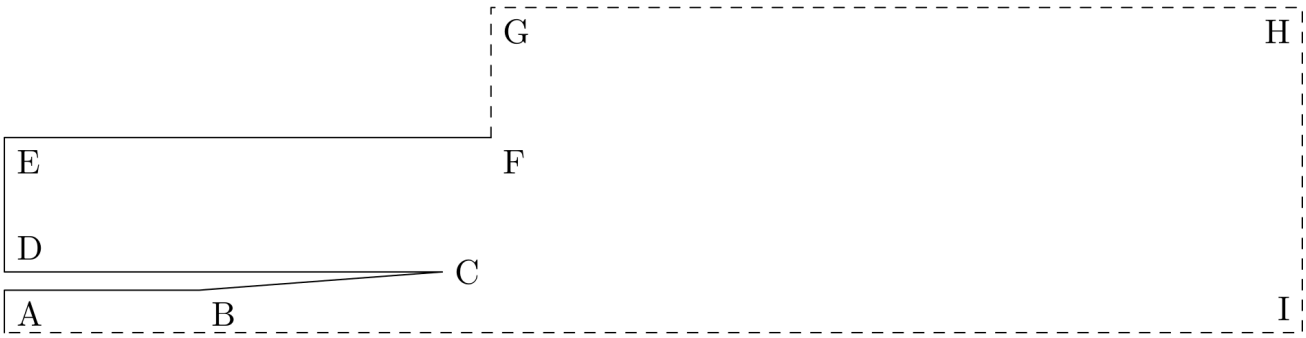

	X (abscissa) (mm)	Y (mm)		X(abscissa) (mm)	Y (mm)
A	-20	1.75	E	-20	8
B	-12	1.75	F	0	8
C	-2	2.5	G	0	40
D	-20	2.5	H	100	40

Figure 9: Geometrical data for half the computational domain of the evaporating liquid jet.

The inlet boundary conditions correspond to two subsonic inflows:

– central flow made of pure liquid oxygen, at 100K and 30m/s, pressure 3MPa along segment AB of Fig. 9,

– peripheral flow made of pure gaseous hydrogen, at 150K and 200m/s, with the pressure of 3MPa along segment DE of Fig. 9,

and one subsonic outlet, along segments GH and HI, where a non-reflecting subsonic boundary condition is imposed at 3MPa. The remaining walls are treated as symmetric boundary conditions. The mesh consists of 360 000 triangles, with a spatial discretization varying from 0.1mm in the jet to 0.6mm in the far field.

The small scale destabilization of the liquid jet requires to extend the numerical solver presented in Saurel et al. (2016) [6] to second order. This was achieved following the MUSCL-Hancock scheme with the Superbee limiter, as detailed for example in Toro [14].

Two computations have been carried out on the same mesh, with the aim of studying the effect of the thermochemical relaxation on the jet destabilization. The contours of mass fraction of liquid oxygen as obtained with and without evaporation effects are compared in Figs. 10.a and 10.b, showing serious changes due to the jet evaporation.

As expected, the filaments separating the main liquid core and the gas gradually vanish as a consequence of evaporation, resulting in much steeper contours of liquid mass fraction in the vicinity of the jet, and very few pockets of liquid with significant life time. Fig. 10.d shows the contour of vapor oxygen (which indeed remains at zero in the case without phase transfer). Fig. 10.c plots the total oxygen mass fraction contour ($Y_1 + Y_2$). It can also be compared to Fig. 10.a

Although the results in terms of total mass fraction for oxygen qualitatively seem close whether or not the mass transfer is activated, it is clear that the vapor mass fraction is of utmost importance for our future work, which shall include the gaseous combustion between vapor oxygen and hydrogen.

Capillary effects are not included in these simulations, as the intense velocity gradients make them negligible in the present jet destabilization conditions. However, capillary effects may be of importance when the filaments start separating from the jet, and our future work will include them, following the strategy presented in Le Martelot et al (2014) [15].

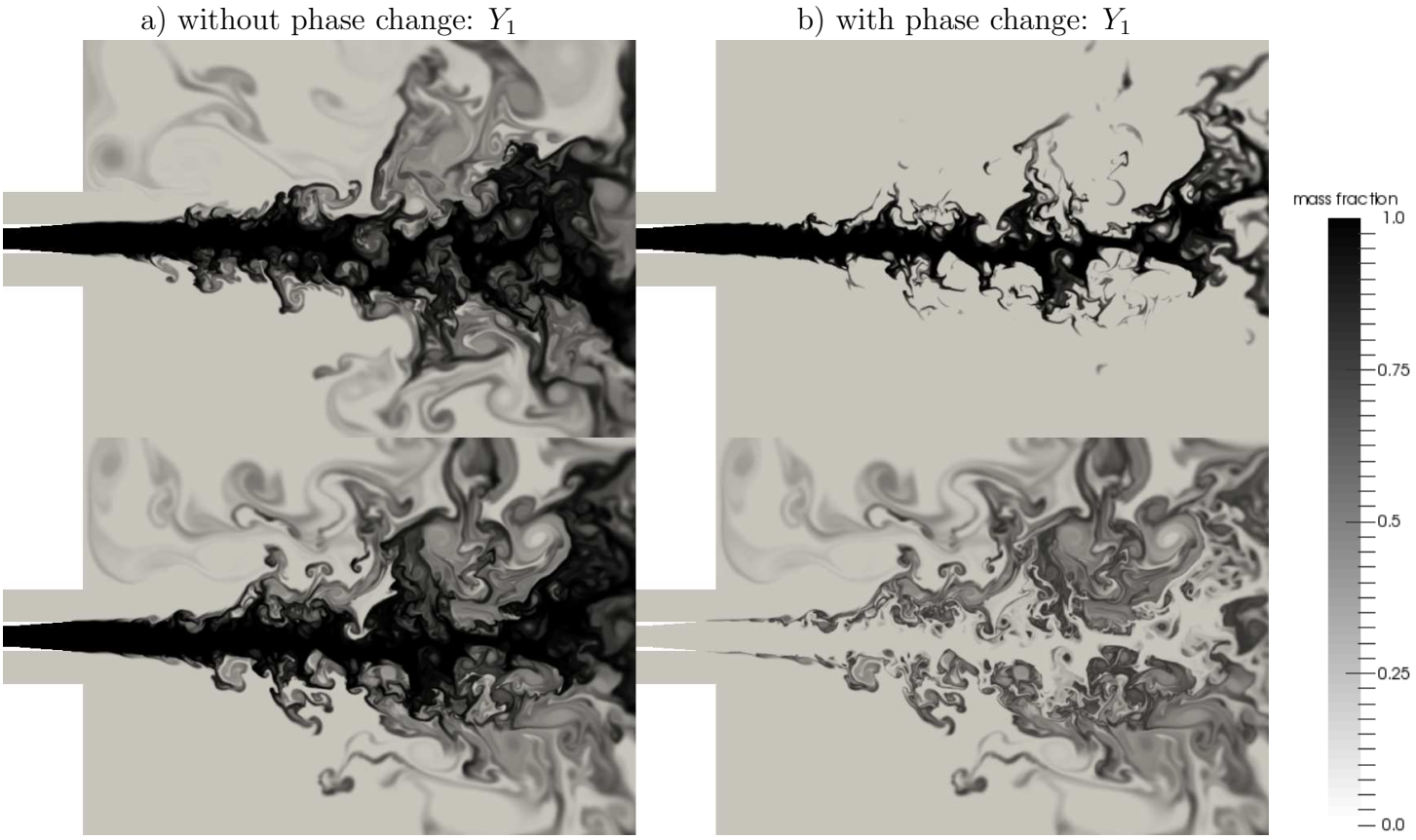

Figure 10: Fragmentation of a liquid O_2 jet by a coaxial high-speed H_2 current. The results from Figs b,c and d are from the same computation, whereas Fig a is taken at the same time, from a computation without phase transition. All results are expressed in terms of mass fraction, on the same color map. Figs a) and b) compare the liquid mass fraction of oxygen without and with phase transfer. Fig. d) shows the contour of vapor oxygen resulting from the liquid jet evaporation. Fig. c) represents the sum $Y_1 + Y_2$ (Fig b+c), showing a total mass fraction of oxygen, to be compared with the case without mass transfer (Fig. a).

8.2. Explosive liquid water dispersal in air

The present relaxation solver has been presented in the context of the 4-equation model. This model considers mechanical and thermal equilibrium but thermochemical disequilibrium. However the relaxation solver is not restricted to such a model and can be extended to non-equilibrium hyperbolic flow models, such as Baer and Nunziato's (1986) [2] and its reduced versions. This last model is a 7-equation model assuming mechanical, thermal and chemical disequilibrium. Thereby, finding local thermodynamic equilibrium requires extra ingredients such as velocity, pressure and temperature relaxation solvers such as the ones promoted in [9, 10]. We propose here to repeat the explosive liquid water dispersal test presented in Furfaro and Saurel (2015) [16] with the 4 and 7-equation models. The test consists in a cylindrical gas-liquid explosion schematically represented in Fig 11. The results are given in Fig 12.

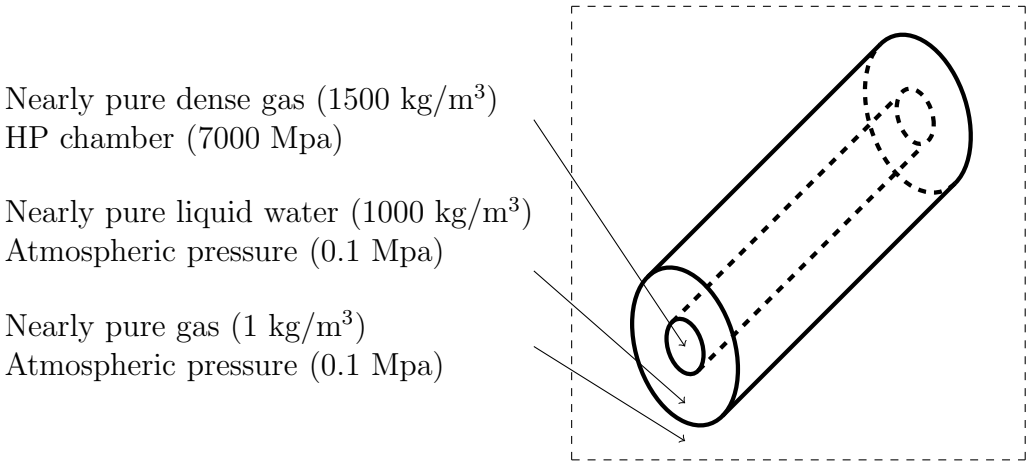

Figure 11: Schematic representation of the cylindrical gas-liquid explosive system. A cylindrical explosive charge is surrounded by a liquid water layer. The internal cylinder is 160 mm long with a 52 mm radius and is initially filled with nearly pure dense gas (1500 kg/m^3) at high pressure (7000 Mpa). The external cylinder is 160 mm long with a 96 mm radius and is initially filled with nearly pure liquid water (1000 kg/m^3) at atmospheric pressure (0.1 MPa). Atmospheric conditions with nearly pure gas (1 kg/m^3) at 0.1 MPa are considered around both cylinders.

No noticeable changes are visible in Fig 12 illustrating the capabilities of the relaxation solver to model phase change in both 7-equation and 4-equation models . An evaporation front is clearly visible with both models.

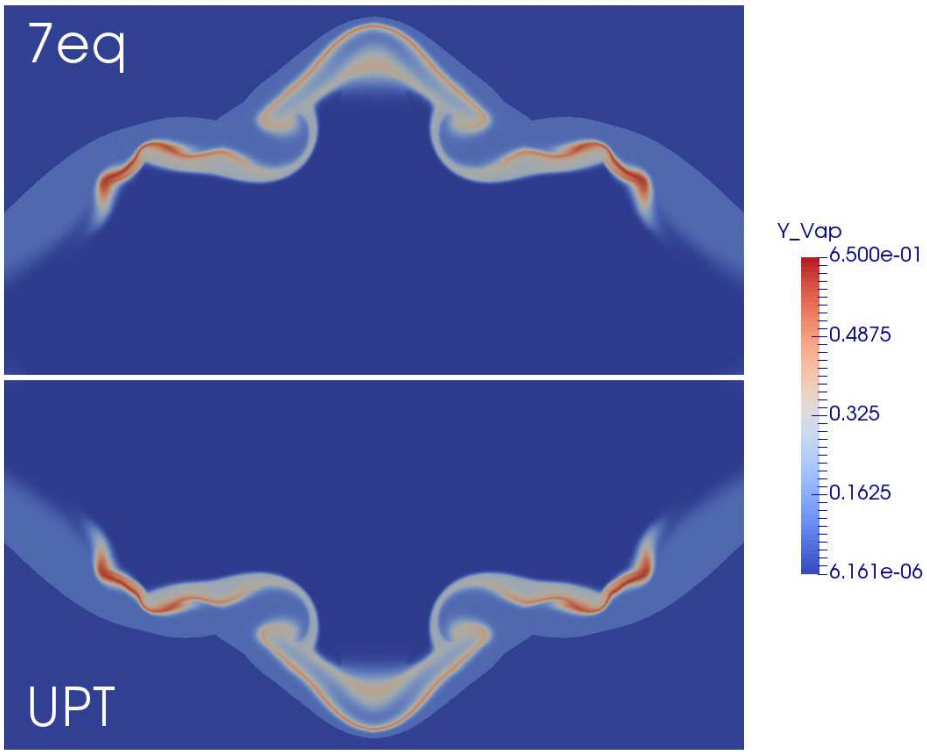

Figure 12: Vapor mass fraction created during a 2D cylindrical gas-liquid explosive dispersl. The figure compares the results obtained with the 4-equation model (mechanical and thermal equilibrium at bottom) and with the 7-equation model (total disequilibrium at top) after relaxation of the pressures, velocities, temperatures following the relaxations solvers presented in [9] and the chemical potential following the relaxation method presented in this paper. The results display no noticeable change.

9. Conclusions

A simple relaxation solver has been built, able to deal with phase transition between a liquid phase, and a multicomponent gas phase. The solver presents substantial advantages compared to iterative methods:

- CPU savings over 50%,
- high simplicity of implementation and verification,
- increased robustness with high-order methods.

This is reached without any noticeable loss of accuracy.

This research can be continued in many directions. Among them, consideration of supercritical fluids in the same theoretical frame appears important. Another perspective deals with the consideration of combustion effects in the gas phase.

References

[1] A. Chiapolino, P. Boivin, R. Saurel, A simple phase transition relaxation solver for multiphase flows., Int. J. for Numerical Methods in Fluids, accepted.

[2] M. Baer, J. Nunziato, A two-phase mixture theory for the deflagration-to-detonation transition (DDT) in reactive granular materials, International Journal of Multiphase Flow 12 (6) (1986) 861–889.

[3] A. Kapila, R. Menikoff, J. Bdzil, S. Son, D. Stewart, Two-phase modeling of deflagration-to-detonation transition in granular materials: Reduced equations, Physics of Fluids 13 (10) (2001) 3002–3024.

[4] R. Saurel, F. Petitpas, R. Abgrall, Modelling phase transition in metastable liquids: application to cavitating and flashing flows, Journal of Fluid Mechanics 607 (2008) 313–350.

[5] S. LeMartelot, B. Nkonga, R. Saurel, Liquid and liquid-gas flows at all speeds, Journal of Computational Physics 255 (2013) 53–82.

[6] R. Saurel, P. Boivin, O. Le Métayer, A general formulation for cavitating, boiling and evaporating flows, Computers and Fluids 128 (2016) 53–64.

[7] P. Downar-Zapolski, Z. Bilicki, L. Bolle, J. Franco, The non-equilibrium relaxation model for one-dimensional flashing liquid flow, International Journal of Multiphase Flow 22 (3) (1996) 473–483.

[8] M. Barret, E. Faucher, J. Hérard, Schemes to compute unsteady flashing flows, AIAA Journal 40 (5) (2002) 905–913.

[9] O. Le Métayer, J. Massoni, R. Saurel, Dynamic relaxation processes in compressible multiphase flows. Application to evaporation phenomena, in: ESAIM: Proceedings, Vol. 40, EDP Sciences, 2013, pp. 103–123.

[10] M. Lallemand, R. Saurel, Pressure relaxation procedures for multiphase compressible flows, INRIA Report 403 (8).

[11] O. Le Métayer, J. Massoni, R. Saurel, Elaborating equations of state of a liquid and its vapor for two-phase flow models; élaboration des lois d'état d'un liquide et de sa vapeur pour les modèles d'écoulements diphasiques, International Journal of Thermal Sciences 43 (3) (2004) 265–276.

[12] O. Le Métayer, R. Saurel, The Noble-Abel Stiffened-Gas equation of state, Physics of Fluids 28 (4) (2016) 046102.

[13] D. Furfaro, R. Saurel, Modeling droplet phase change in the presence of a multi-component gas mixture, Applied Mathematics and Computation 272 (2016) 518–541.

[14] E. F. Toro, Riemann solvers and numerical methods for fluid dynamics: A practical introduction, Springer Science & Business Media, 1997.

[15] S. Le Martelot, R. Saurel, B. Nkonga, Towards the direct numerical simulation of nucleate boiling flows, International Journal of Multiphase Flow 66 (2014) 62–78.

[16] D. Furfaro, R. Saurel, A simple HLLC-type Riemann solver for compressible non-equilibrium two-phase flows, Computers and Fluids 111 (2015) 159–178.

AppendixA. Summary of the iterative algorithm

The algebraic system to be solved is,

$$\begin{cases} v = Y_1^* v_1(p^*, T^*) + Y_2^* v_2(p^*, T^*) + \sum_{k \geqslant 3} Y_k v_k(p^*, T^*), \\ e = Y_1^* e_1(p^*, T^*) + Y_2^* e_2(p^*, T^*) + \sum_{k \geqslant 3} Y_k e_k(p^*, T^*), \\ p_{sat}(T^*) = \left(\dfrac{\frac{Y_2^*}{W_2}}{\frac{Y_2^*}{W_2} + \sum_{k \geqslant 3} \frac{Y_k}{W_k}} \right) p^*, \end{cases} \tag{A.1}$$

where the superscript * denotes the thermodynamic equilibrium state. Since $Y_1 = 1 - Y_2 - \sum_{k\geqslant 3} Y_k$, the algebraic system reads,

$$\left\{\begin{array}{l} f_1(p^*,T^*,Y_2^*) = v - \left(1 - Y_2^* - \displaystyle\sum_{k\geqslant 3} Y_k\right) v_1(p^*,T^*) - Y_2^* v_2(p^*,T^*) - \displaystyle\sum_{k\geqslant 3} Y_k v_k(p^*,T^*), \\ f_2(p^*,T^*,Y_2^*) = e - \left(1 - Y_2^* - \displaystyle\sum_{k\geqslant 3} Y_k\right) e_1(p^*,T^*) - Y_2^* e_2(p^*,T^*) - \displaystyle\sum_{k\geqslant 3} Y_k e_k(p^*,T^*), \\ f_3(p^*,p_{sat}^*,Y_2^*) = p_{sat}^* - \left(\dfrac{\frac{Y_2^*}{W_2}}{\frac{Y_v^*}{W_2} + \sum_{k\geqslant 3}\frac{Y_k}{W_k}}\right) p^*. \end{array}\right. \tag{A.2}$$

However the relation between $p_{sat}(T^*)$ and T^*,

$$\ln\left(p_{sat} + p_{\infty,v}\right) = A + \frac{B + E\, p_{sat}}{T_{sat}} + C\ln\left(T_{sat}\right) + D\ln\left(p_{sat} + p_{\infty,l}\right), \tag{A.3}$$

is non-linear and no analytical relation can be found. An additional equation is consequently added to Syst (A.2).

It is convenient to use a reference state defined with the others NASG or SG coefficients which have been determined via theoretical equations and experimental data (see LeMétayer et al [11], [12]). Let us define,

$$\left\{\begin{array}{l} T_0 = \dfrac{q_1 - v_2}{C_{p,2} - C_{v,2}} = \dfrac{B}{C}, \\ p_0 = \dfrac{\left(C_{p,2} - C_{v,2}\right) p_{\infty,1} - \left(C_{p,1} - C_{v,1}\right) p_{\infty,2}}{\left(C_{p,1} - C_{v,1}\right) - \left(C_{p,2} - C_{v,2}\right)} = \dfrac{p_{\infty,1} - D p_{\infty,2}}{D - 1}. \end{array}\right. \tag{A.4}$$

Eq (A.3) is now written with the built reference state p_0, T_0,

$$\ln\left(p_0 + p_{\infty,2}\right) = A + \frac{B + E\, p_0}{T_0} + C\ln\left(T_0\right) + D\ln\left(p_0 + p_{\infty,1}\right). \tag{A.5}$$

Subtracting Eq. (A.5) to Eq. (A.3), it is straight-forward to find another formulation connecting the saturation pressure and temperature,

$$\frac{p_{sat} + p_{\infty,2}}{p_0 + p_{\infty,2}} = \exp\left\{C\Big[\frac{T_0}{T_{sat}} + \ln\left(\frac{T_{sat}}{T_0}\right) - 1\Big]\right\}\left(\frac{p_{sat} + p_{\infty,1}}{p_0 + p_{\infty,1}}\right)^D \exp\left\{E\left(\frac{p_{sat}}{T_{sat}} - \frac{p_0}{T_0}\right)\right\}. \tag{A.6}$$

The algebraic system thus reads,

$$\begin{cases} f_1(p^*,T^*,Y_2^*) = v - \left(1 - Y_2^* - \sum_{k\geqslant 3} Y_k\right) v_1(p^*,T^*) - Y_2^* v_2(p^*,T^*) - \sum_{k\geqslant 3} Y_k v_k(p^*,T^*), \\ f_2(p^*,T^*,Y_2^*) = e - \left(1 - Y_2^* - \sum_{k\geqslant 3} Y_k\right) e_1(p^*,T^*) - Y_2^* e_2(p^*,T^*) - \sum_{k\geqslant 3} Y_k e_k(p^*,T^*), \\ f_3(p^*,p_{sat}^*,Y_2^*) = p_{sat}^* - \left(\dfrac{\frac{Y_2^*}{W_2}}{\frac{Y_2^*}{W_2} + \sum_{k\geqslant 3}\frac{Y_k}{W_k}}\right) p^*, \\ f_4(p_{sat}^*,T^*) = \dfrac{p_{sat}^* + p_{\infty,2}}{p_0 + p_{\infty,2}} - \exp\left\{C\Big[\dfrac{T_0}{T^*} + \ln\left(\dfrac{T^*}{T_0}\right) - 1\Big]\right\}\left(\dfrac{p_{sat}^* + p_{\infty,1}}{p_0 + p_{\infty,1}}\right)^D \exp\left\{E\left(\dfrac{p_{sat}^*}{T^*} - \dfrac{p_0}{T_0}\right)\right\}. \end{cases} \tag{A.7}$$

Four variables are unknown, p^*, T^*, Y_v^*, p_{sat}^* and System (A.7) is non-linear calling for an iterative method such as Newton-Raphson's. Let us then denote,

$$X = \begin{pmatrix} p^* \\ T^* \\ Y_v^* \\ p_{sat}^* \end{pmatrix}, \quad F(X) = \begin{pmatrix} f_1(p^*,T^*,Y_2^*)) \\ f_2(p^*,T^*,Y_2^*) \\ f_3(p^*,p_{sat}^*,Y_2^*) \\ f_4(p_{sat}^*,T^*) \end{pmatrix}. \tag{A.8}$$

The system $F(X) = 0$ has to be resolved. Its solution is given by,

$$X^n = X^{n-1} - J\Big\{F(X^{n-1})\Big\}^{-1} F(X^{n-1}), \tag{A.9}$$

with n denoting the current iteration and $J\Big\{F(X^{n-1})\Big\}^{-1}$ the inverse of the Jacobian matrix,

$$J(f_1,f_2,f_3,f_4) = \begin{pmatrix} \frac{\partial f_1(p^*,T^*,Y_2^*)}{\partial p^*} & \frac{\partial f_1(p^*,T^*,Y_2^*)}{\partial T^*} & \frac{\partial f_1(p^*,T^*,Y_2^*)}{\partial Y_2^*} & \frac{\partial f_1(p^*,T^*,Y_2^*)}{\partial p_{sat}^*} \\ \frac{\partial f_2(p^*,T^*,Y_2^*)}{\partial p^*} & \frac{\partial f_2(p^*,T^*,Y_2^*)}{\partial T^*} & \frac{\partial f_2(p^*,T^*,Y_2^*)}{\partial Y_2^*} & \frac{\partial f_2(p^*,T^*,Y_2^*)}{\partial p_{sat}^*} \\ \frac{\partial f_3(p^*,p_{sat}^*,Y_2^*)}{\partial p^*} & \frac{\partial f_3(p^*,p_{sat}^*,Y_2^*)}{\partial T^*} & \frac{\partial f_3(p^*,p_{sat}^*,Y_2^*)}{\partial Y_2^*} & \frac{\partial f_3(p^*,p_{sat}^*,Y_2^*)}{\partial p_{sat}^*} \\ \frac{\partial f_4(p_{sat}^*,T^*)}{\partial p^*} & \frac{\partial f_4(p_{sat}^*,T^*)}{\partial T^*} & \frac{\partial f_4(p_{sat}^*,T^*)}{\partial Y_v^*} & \frac{\partial f_4(p_{sat}^*,T^*)}{\partial p_{sat}^*} \end{pmatrix} \tag{A.10}$$

In order to gain accuracy and robustness, it is convenient to write Eq. (A.9) as,

$$\begin{cases} J(F(X^{n-1}))\triangle X = -F(X^{n-1}), \\ \triangle X = X^n - X^{n-1}. \end{cases} \tag{A.11}$$

Thereby, for a given X, a linear system is found and the variation $\triangle X$ can be determined via a direct method such as the Gaussian elimination or an iterative one such as Gauss-Seidel's. The variables are then updated as,

$$X^n = \triangle X + X^{n-1}. \tag{A.12}$$

A solution is obtained when $\triangle X < \epsilon$ or alternatively when $|f_1| < \epsilon$, $|f_2| < \epsilon$, $|f_3| < \epsilon$, $|f_4| < \epsilon$, with $\epsilon \to 0$.

This procedure is robust and accurate. It is used in all test problems of Section 6.